Ionics (2020) 26:3893–3900
https://doi.org/10.1007/s11581-020-03549-x

ORIGINAL PAPER

Mechanical strong polymer cross-linking PVDF nanofiber electrolyte for lithium-ion batteries

Fenglin Zhou[1] · Haiyang Liao[1] · Zhanzhan Zhang[1]

Received: 3 February 2020 / Revised: 26 March 2020 / Accepted: 28 March 2020 / Published online: 15 April 2020

Abstract

Solid-state battery has been considered as ultimate form of lithium-ion batteries due to high safety and extreme temperature tolerance, but the solid-state electrolyte fails to meet the requirements which are often suffered from low ionic conductivity, weak mechanical properties, and poor interfacial contact with the electrode simultaneously. In this paper, we report preparation of a new polymer cross-linking PVDF nanofibrous-based quasi solid-state electrolyte (P-PVDF) by in situ polymerization of melamine and epoxy-ended amino-terminated polyoxypropylene with $LiPF_6$-based liquid electrolyte in framework of PVDF nanofiber. The polymer cross-linking PVDF nanofiber not only improves mechanical strength for polymer electrolyte but also contributes to the one-off formation of a homogenous solid electrolyte interface to suppressing dendrite lithium. The ether-dominated polymer chains provide ionic transportation channel induced high ionic conductivity (1.35 mS/cm). In comparison with liquid electrolyte, the P-PVDF polymer electrolyte exhibits significantly enhanced rate behavior with retention rate of 75% (61% for the liquid elelctrolyte) at 8 °C, cycling stability of 92% initial capacities (80% for liquid electrolyte) after 200 cycles.

Keywords Lithium-ion batteries · Quasi solid-state electrolyte · Dendrites-free

Introduction

The overwhelming development in electronic device such as flexible electronic skin, portable electronic tools, and electric vehicles has tremendous impact on Today's life [1–6]. This influence is met the demand of revolutionized the development of lithium-ion batteries [7–10]. However, the state-of-the-art lithium-ion batteries, which contained highly flammable and volatile organic liquid electrolyte, are suffered from serious safety problems (leakage, fire, weak solid electrolyte interface (SEI), and explosions), and that are difficult to meet the safety issues and specific energy requirements for future electronic devices [11–16]. Generally, the inhomogeneous SEI layer has been considered as a reason which results in the unstopped formation of lithium dendrites. Based on this, a highly uniform and stable SEI layer plays a critical role on stabilizing current flux and suppressing lithium dendrite growth, thus improving CE and long-term cycle lifespan [17–19]. However, traditional liquid electrolyte (LE) cannot meet the requirement as existence of undesirable side reaction with lithium metal. Therefore, replacement of the LE can be considered as the most convenient and effective method for addressing the drawbacks. As a promising substitute with LE, the usages of solid electrolyte can effectively resolve the above safety problems due to stability with electrode and exhibiting significantly suppress the lithium dendrite growth.

It is well-known that solid electrolyte is mainly divided into three categories: inorganic solid electrolyte (ISE) [20], all-solid-state polymer electrolyte (SPE) [21], and gel polymer electrolyte (GPE) [22]. ISE gives a poor interfacial compatibility with electrode and electrochemical performance at room temperature even though its deliveries a high ionic conductivity ($> 10^{-4}$ S/cm), the working temperature for ISE type electrolyte often requires up to 50 °C. In case of SPE, it has optimized interfacial property, highly flexibility, and robust mechanical property compared with ISE but fails to ionic conductivity ($< 10^{-4}$ S/cm) [23]. Taking full advantage of ISE and SPE, the performances of ionic conductivity and interfacial issues are improved for GPE. Nevertheless, the improved

Electronic supplementary material The online version of this article (https://doi.org/10.1007/s11581-020-03549-x) contains supplementary material, which is available to authorized users.

✉ Haiyang Liao
haiyangliao1990@163.com

[1] School of Mechanical Engineering, Hunan University of Technology, Zhuzhou 412007, China

performances are sacrificed by mechanical strength. All of these restrict the practical usage in lithium-ion batteries. In this regard, a GPE with duel network (DN) can significantly address the problems of solid-state batteries. The LE trapped in the solid polymer matrix can improve electrochemical performance, ionic conductivity, and mechanical properties because beneficial from LE and framework materials.

A consecutive pore structure is favorable to ion transportation and trapping more LE, which is regarded as an ideal scaffold for immobilization of LE. Much different types of LE host materials have been reported such as most potential host materials poly (ethylene oxide) (PEO), poly (vinylidene fluoride) (PVDF), and poly (vinylidene fluoride-hexafluoropropylene) (PVDF-HFP) [24, 25]. Among these host materials, PVDF and PVDF-HFP are regarded as most suitable materials for encapsulation of LE because that it possesses the high dielectric constant, thus promoting the dissociation of lithium salts.

In this paper, we report preparation of a new polymer cross-linking PVDF nanofibrous-based quasi solid-state electrolyte (P-PVDF) to improve interfacial resistance between electrolyte and electrodes. P-PVDF is prepared by in situ polymerization of melamine and epoxy-ended amino-terminated polyoxypropylene in PVDF nanofiber framework, using $LiPF_6$-based LE as solvent. The connected PVDF nanofiber framework can significantly improve mechanical strength comparing to single network PVDF nanofiber electrolyte, while ether-based cross-linking polymer chains endue fast ion transportation. Meanwhile, the hybrid network PVDF nanofiber electrolyte contributes to the one-off formation of a homogenous SEI to suppressing dendrite lithium. The assembled $LiFePO_4$-based cell using P-PVDF as electrolyte exhibits significantly enhanced rate behavior with retention rate of 75% at 8 °C and cycling stability of 92% initial capacities after 200 cycles.

Experimental

Preparation of P-PVDF nanofiber polymer electrolytes The amino-terminated polyoxypropylene (NH_2-PPE, Mn = 2000, Shanghai Macklin Biochemical CO., Ltd., Shanghai) and poly (ethylene glycol) diglycidyl ether (PEDE, Mn = 400, Shanghai Macklin Biochemical CO., Ltd., Shanghai) are dissolving in ethanol. The molar radio of amino and epoxy keeps 1:2 for ensuring adequate epoxy and acquiring epoxy-ended chain extender. The reaction wormed at 50 °C for 2 h, and the product was collected by removing the solvents, named epoxy-ended PPE. The P-PVDF polymer electrolytes were prepared by in situ polymerization of precursor solution in the framework of PVDF nanofiber. The precursor consisted of 2 vol% epoxy-ended PPE and various contents of melamine ($vol._{melamine}$:$vol._{epoxy\text{-}ended\ PPE}$, 2%, 5%, and 10%) dissolved into 2 ml $LiPF_6$ electrolyte (1 M $LiPF_6$ salt in a non-aqueous mixture of EC/DEC/EMC (1:1:1 by volume), Zhangjiagang Guotai-Huarong New Chemical Materials Co., Ltd., Jiangsu). Subsequently, the precursor solution injected into a piece of PVDF nanofiber membrane (diameter = 18 mm, fabricated by electro-spinning technique as previous work [26]) and heated to 80 °C for 6 h to obtain P-PVDF. The P-PVDF polymer electrolyte contained different contents of melamine were denoted P_n-PVDF. All procedures were carried out in Ar-filled glove box ($H_2O < 0.1$ ppm, $O_2 < 0.1$ ppm).

Cell assembly $LiFePO_4$-based cathode was prepared by casting a mixture of $LiFePO_4$ powders (Shenzhen Kejing Star Technology Co., Ltd., Shenzhen, China), carbon black (Super-P), and PVDF as binder by a weight ratio of 80:10:10 on Al foil. The electrodes were first punched into circles (D = 14 mm) with the loading content of the $LiFePO_4$ being ~ 2.0 mg/cm and subsequently kept in a vacuum oven at 80 °C for 48 h. The lithium metal foil (battery grade, D = 16 mm, thickness = 2 mm, Shenzhen Kejing Star Technology Co., Ltd., Shenzhen, China) was used as the anode. To assemble $LiFePO_4$-based cell using P_2-PVDF as polymer electrolyte, the batteries sealed in CR2025 coin cell. The symmetric cells of double stainless steel (SS) and lithium systems were assembled by sandwiching the P_n-PVDF between two pieces of SS or lithium metal foil in a CR2025 coin cell. Lithium//P_n-PVDF//SS cells were assembled by equipping P_n-PVDF between lithium metal foil and SS in CR2025 coin cell. The whole process for the cell assembly was carried out in an Ar-filled glove box ($H_2O <$ 0.1 ppm, $O_2 < 0.1$ ppm).

Characterization of P-PVDF polymer electrolyte The morphology of the obtained samples was observed by scanning electron microscopy (SEM, SN-3400, Hitachi Ltd., Japan). Fourier-transform infrared spectroscopy (FT-IR) was recorded on a Nicolet 6700 spectrometer from 4000 to 500 cm^{-1}. Tensile strength of P-PVDF was carried out on the mechanical testing system (Zwick-Roell Z005, Ulm, Germany) at strain rate of 1 mm/min and the initial gauge length was 20 mm. Electrochemical performances were investigated on electrochemical working station (CHI 660E, CH. Instruments Inc. Shanghai, China). The ionic conductivity was obtained from following equation:

$$\sigma = L/R_b A \quad (1)$$

where the L and A are representative of the thickness and the effective area of the separator, respectively. A LAND battery cycle system (Wuhan Blue Electric Co., Ltd., Wuhan, China) was employed to investigate the battery performances (charge-discharge and cycling performance) of cells.

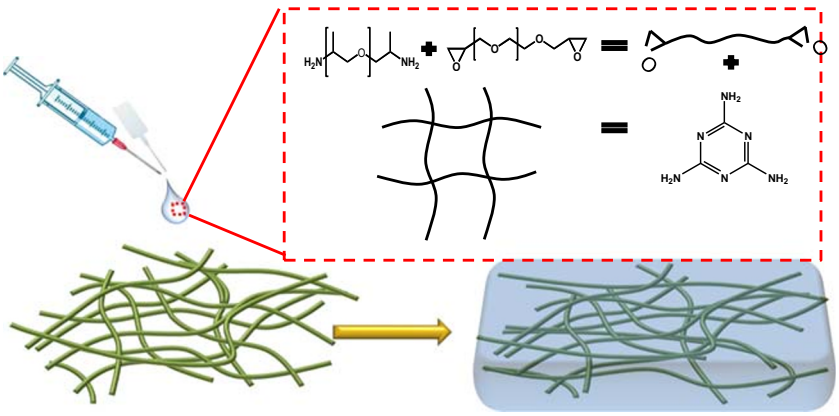

Fig. 1 Polymerization mechanism of the cross-linking polymer

Results and discussion

The mechanism of cross-linked polymer is shown in Fig. 1. Firstly, the NH_2-PPE reacted with PEDE to achieve two epoxy groups. Subsequently, the two epoxy groups reacted with three amino groups on the melamine through ring-opening polymerization, further growing into bulk polymer. The mechanism of polymerization is verified by FT-IR, as shown in Fig. 2a. The bands of 1654 cm^{-1} (N-H), 1024 cm^{-1} (C-O), and 885 cm^{-1} (epoxy group) are assigned to epoxy-ended PPE. Melamine is confirmed by the bands of 1651 cm^{-1} and 1554 cm^{-1} which are corresponding to N-H and C=N groups. The band at 885 cm^{-1} (epoxy group) is disappeared, while the band of 1554 cm^{-1} which belongs to C=N groups of melamine is detected after polymerization, suggesting cross-linking polymer successfully synthesized. Mechanical toughness not only deliveries to maintain membrane-state but also prevents physical damage during assembling process and suppresses dendrite lithium. Figure 2b presents stress-strain curves of pure PVDF and P_n-PVDFs. Nevertheless, the pure PVDF nanofiber membrane gives poor mechanical strength (0.04 Mpa). The mechanical properties enhance with increasing cross-linking intensity of polymer, and finally deliveries 0.2 Mpa for P_{10}-PVDF. The increased mechanical strength is attributed to cross-linking polymer enhanced nanofiber.

The morphology of as-prepared polymer electrolyte is displayed in Fig. 3. The morphology of pure PVDF nanofiber membrane exhibits random aggregation of fibrous structure (Fig. 3a). Much difference from loose structure of pure PVDF nanofiber membrane, the cross-linking polymer fills up the volume of PVDF nanofiber and further connects each other into a compact structure (Fig. 3b). From EDXS elemental mapping, C and F signals recording in P-PVDF which are characteristic elemental of PVDF are maintained nanofibrous structure, the N signal also consistently distributes in P-PVDF which are stemmed from the group of –NH group in cross-linking polymer, suggesting existence of cross-linking polymer.

The plots of log σ vs. T^{-1} for as-prepared P-PVDF polymer electrolyte present in Fig. 4a. The ionic conductivity of pure PVDF is as high as P_2-PVDF, reaching value of 1.35 mS/cm at 25 °C. That value is much higher than LE which only gives 0.95 at 25 °C (see Fig. S1a). However, the contents of melamine further increasing, the ionic conductivity dramatically reduced to 0.74 mS/cm (P_5-PVDF) and 0.53 mS/cm (P_{10}-PVDF), indicating that the suitable immobilization of melamine for P-PVDF polymer electrolyte is about 2%. The decreased ionic conductivity is attributed to cross-linking intensity. In high cross-linking intensity, the mobility of polymer chains are impeded; as a result, the movement of ion is

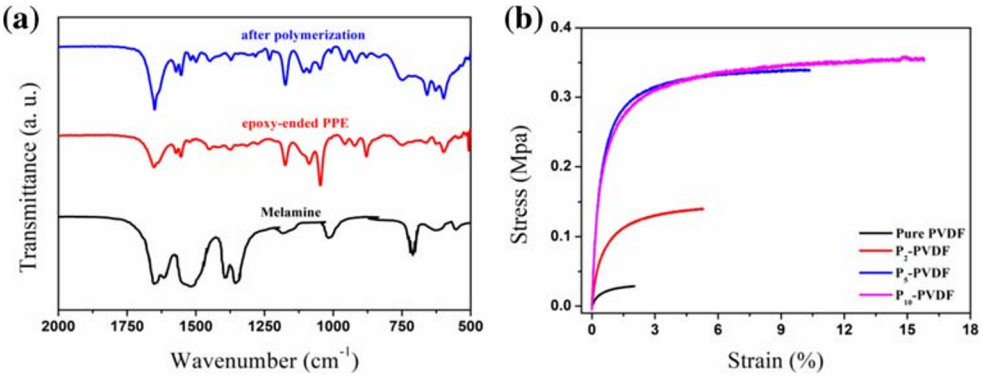

Fig. 2 **a** FT-IR spectra of monomer and cross-linking polymer; **b** stress-strain curves of pure PVDF and P_n-PVDFs

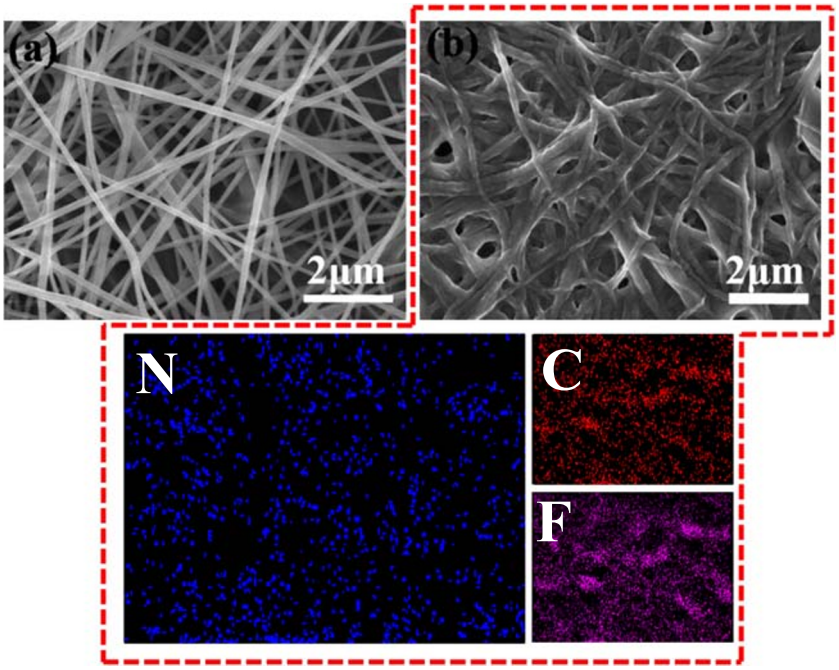

Fig. 3 Morphology of pure PVDF and P-PVDF

hindered by the ponderous polymer chains. The activation energy (E_a) refers to ionic transportation. The lower value of E_a means rapid ionic transportation. The E_a is calculated from Vogel-Tamman-Fulcher (VTF) empirical equation [27]:

$$\sigma = \sigma_0 T^{-1/2} \exp\left(-\frac{E_a}{R(T-T_0)}\right) \quad (2)$$

where E_a is the activation energy, σ_0, T_0, and R are constant factors for the pre-exponential factor, parameter corrected to the gas transition temperature and ideal gas constant, respectively. The results are similar with ionic conductivity. The P_2-PVDF polymer electrolyte exhibits minimum E_a ($\sim 2.3 \times 10^{-2}$ eV) that much lower than other polymer electrolytes ($\sim 3.2 \times 10^{-2}$ eV for pure PVDF, 4.3×10^{-2} eV for LE, 4.8×10^{-2} eV for P_5-PVDF, 5.5×10^{-2} eV for P_{10}-PVDF). This means the ion could easily transmitted in the P_2-PVDF electrolyte. The remarkable E_a are originated from ether-dominated cross-linking polymer. The ether group is intimate with LE, which means more LE are trapped in the ether-dominated cross-linking polymer network. Therefore, the cross-linking polymer immobilization of LE is acted as "lithium-ion tank" which storages into the PVDF nanofiber framework. For the lithium-ion batteries, we prefer to cation (lithium ion) transportation in the batteries system, rather than anion transmitting due to mechanism of lithium-ion batteries. Based on this, lithium-ion transference number (t_+) plays a critical role to evaluate whether the electrolyte could apply in lithium-ion batteries. As seen in Fig. 4b. Comparing with LE (0.32, see Fig. S1b), P_5-PVDF (0.24) and P_{10}-PVDF (0.19), the pure PVDF and P_2-PVDF electrolyte gives relatively high t_+, which achieves as high as 0.36 and 0.48, respectively. It depends on synergistic effect of polymer chains to migrate lithium ion. The –F group in the PVDF could bond with lithium ion, thus the lithium ion could migrate with PVDF polymer chains. In the P-PVDF electrolyte, ether-dominated cross-linking polymer chains have noticeable compatibility with lithium ion; hence, the lithium-ion movement could be significantly improved by double transport network

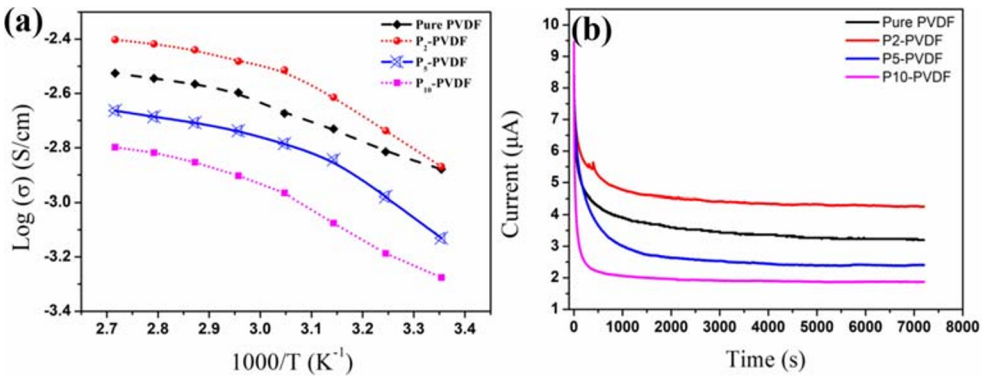

Fig. 4 **a** Arrhenius plots of a polymer electrolyte based on the pure PVDF and P_n-PVDF; **b** chronoamperometry profiles of the pure PVDF and P_n-PVDF at 25 °C, using a step potential of 10 mV

(PVDF and ether-rich cross-linking polymer). In case of high melamine, the ether-rich polymer chains are highly cross-linked by melamine, as consequence of poor chain mobility. The ponderous polymer chain significantly impeded lithium-ion transportation in the electrolyte, thus resulting in low t_+. These illustrate the suitable cross-linking intensity should keep the melamine content at 2%.

The lithium plating/stripping cycling for the cell based on P_2-PVDF polymer electrolyte was tested by using lithium metal symmetric cell. The symmetric lithium cell based on P_2-PVDF as electrolyte gives a low voltage hysteresis ~ 86 mV at 1 mA/cm^2 (Fig. 5a). It is noteworthy that no evidence voltage drop have been occurred even the cycling after 300 h, as indication of good performance on controlling dendrite lithium growth. However, in the case of LE-based symmetric lithium cell, the voltage hysteresis is as high as ~ 190 mV at initial stage much higher than that of P_2-PVDF (Fig. S2a). The voltage hysteresis further increases as the cyclic number gaining and finally stops at 400 mV, presenting poor stability of plating/stripping performance. The poor stability indicates rapid lithium dendrite growth on the surface of lithium metal. The improved dendrite resistance for P_2-PVDF is attributed to formation of homogeneous SEI layer, which is further confirmed by SEM and XPS. In the Fig. 5b, the morphology of the SEI layer formed by P_2-PVDF presents a smooth and flat without any defects, suggesting no obvious rigid dendrite lithium forming. Much contrast with SEI layer formed by P_2-PVDF, the surface of lithium metal becomes much rough and irregularity with visible of agglomerate dendrites for the LE-based cell (as seen in Fig. S2b). The results are stemmed from superior compatibility between P_2-PVDF and lithium electrode. It is further verified by electrochemical impedance spectroscopy (EIS, as shown in Fig. S3). The Nyquist plot for P_2-PVDF exhibits a typical semicircle. The high-frequency semicircles are assigned of the charge transfer resistance on the electrode/electrolyte interfaces. The initial interfacial resistance of the lithium//P_2-PVDF//lithium is ~ 165 Ω. The resistances are positive correlation with the storage time for the cells, owing to active reactions between the interface of bared lithium and electrolyte. The dramatically increased resistances mean inevitable and overwhelming side reactions is occurring. For the cell based on P_2-PVDF as electrolyte, the resistance shows a negligible change (~ 75 Ω increased) even when the storage time lasted for 10 days, as an indication of superior compatibility between P_2-PVDF and lithium metal [28–30]. For confirming the chemical composition of SEI, the chemical structure of SEI layer was confirmed by XPS. The high-resolution C 1s spectra of SEI formed by P_2-PVDF divided into four peaks which locates at 284.3, 286.7, 288.6, and 290.5 eV, corresponding to C-C, C-O, C=O, and RO-COO, respectively (in Fig. 5c). The existence of RO-COO reflects decomposition of organic solvents of liquid electrolyte. A low concentration of RO-COO can be found in the C 1s spectra, indicating formation of ultra-stable SEI layer. Three peaks around 684.5, 686.3, and 688.7 eV can be observed from F 1s spectra (Fig. 5d), reflecting the formation of Li-F $Li_xPO_YF_Z$, and –CF3, respectively. The concentration of $Li_xPO_YF_Z$ and $–CF_3$ are much lower than that of LiF. The SEI layer has more LiF, considering more efficiently suppress the growth of dendrite lithium. In case of the LE-based cell, the concentration of C-O group in the C 1s is lower than that of the C-C group, as presented in Fig. S2c. It indicates the compositions of SEI for the LE-formed are mainly consist of inorganic lithium salts, which is reported in our previous work [31]. It is also can be seen from F 1s XPS spectra for SEI layer formed by liquid electrolyte. A visible concentration of lithium salts (686.5 eV, in Fig. S2d) can be observed, further confirming the inorganic salts-dominated SEI layer. Moreover, the peak intensity of $–CF_3$ is much lower than that of LiF in the SEI layer formed by the P_2-

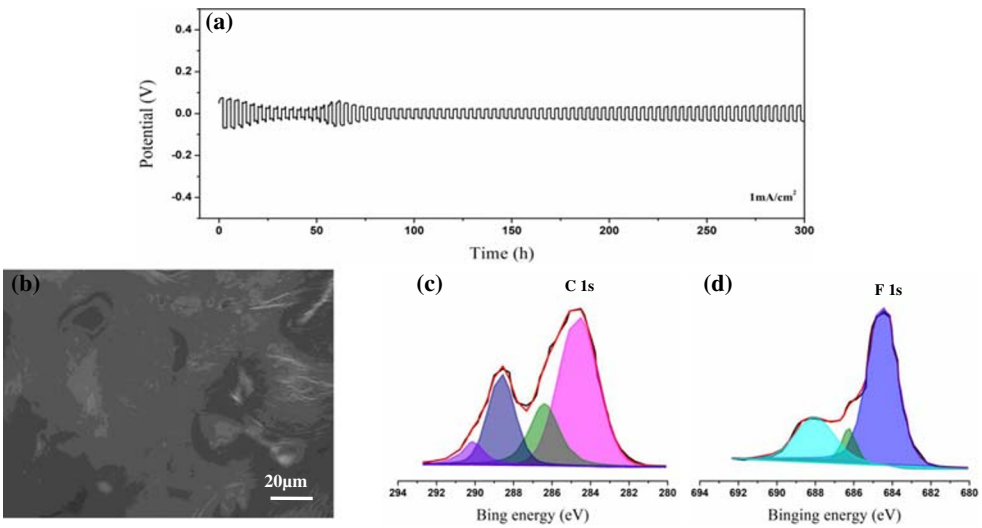

Fig. 5 **a** Long-term lithium plating/stripping cycling of the cell based on P_2-PVDF; **b** morphology of SEI layer formed by the cell using P_2-PVDF as electrolyte; XPS spectra of SEI layer **c** C 1s and (d) F 1s

PVDF. The inorganic salts-based SEI layer is very fragile and unstable, resulting in ongoing consuming lithium ion to "repairing" SEI layer.

To evaluate the practical usage of P_2-PVDF electrolyte, the full cell based on $LiFePO_4$//P_2-PVDF//lithium are assembled and investigated by series of electrochemical performance, as shown in Fig. 6. Figure 6a presents the initial charge/discharge curves of the cell based on LE and P_2-PVDF with potential from 2.75 to 4.2 V. A 0.1 C (25 mA/g) current density carried out for the cell. A couple of electrochemical platform for $LiFePO_4$ (3.45 V for charge, 3.35 V for discharge) relates to oxidation and reduction potential. The specific charge/discharge capacities of P_2-PVDF based cell are 159.5 and 158.6 mAh/g slightly higher than the cell based on LE which gives 158 and 157 mAh/g; respectively. The rate behavior is essential for rapid charge/discharge performance. Figure 6 b profiles the discharge capacity of the cell based on P_2-PVDF at different current density (0.1 C, 0.5 C, 1 C, 3 C, 5 C, and 8 C). In case of relative low current density (0.1 C), the discharge capacity is as high as ~ 160 mAh/g for both cells based on LE (see Fig. S3a) and P_2-PVDF (see Fig. 6b). Increasing current density, the discharge capacity drops for the both cell. Obviously, 75% of initial capacity is still maintained for the cell equipping P_2-PVDF as electrolyte after running at 8 C, the value is much higher than that of the cell assembled LE which only keeps 61% of initial capacity (Fig. S4a). The obtained results are almost higher than that of most recently reported polymer electrolyte (Table S1), as indication of a strong potential for applying in high-performance rechargeable lithium-ion batteries. The superior rate behavior is owed to contribution of high ionic conductivity and remarkable t_+. Consideration of remarkable lithium plating/stripping loop, the as-assembled full cell also exhibits noticeable cyclic lifespan. In Fig. 6c, no evidence capacity fading have been observed after the cell performed 200 cycles, the specific capacity is as high as ~ 139 mAh/g, meaning that 92% of initial capacity is still retained. Moreover, the Coulombic efficiency for each cycle are high than 98%. Much contrast from the cell using P_2-PVDF as electrolyte, it is only 80% of initial capacity maintained after 200 cycles for the LE-based cell, and the

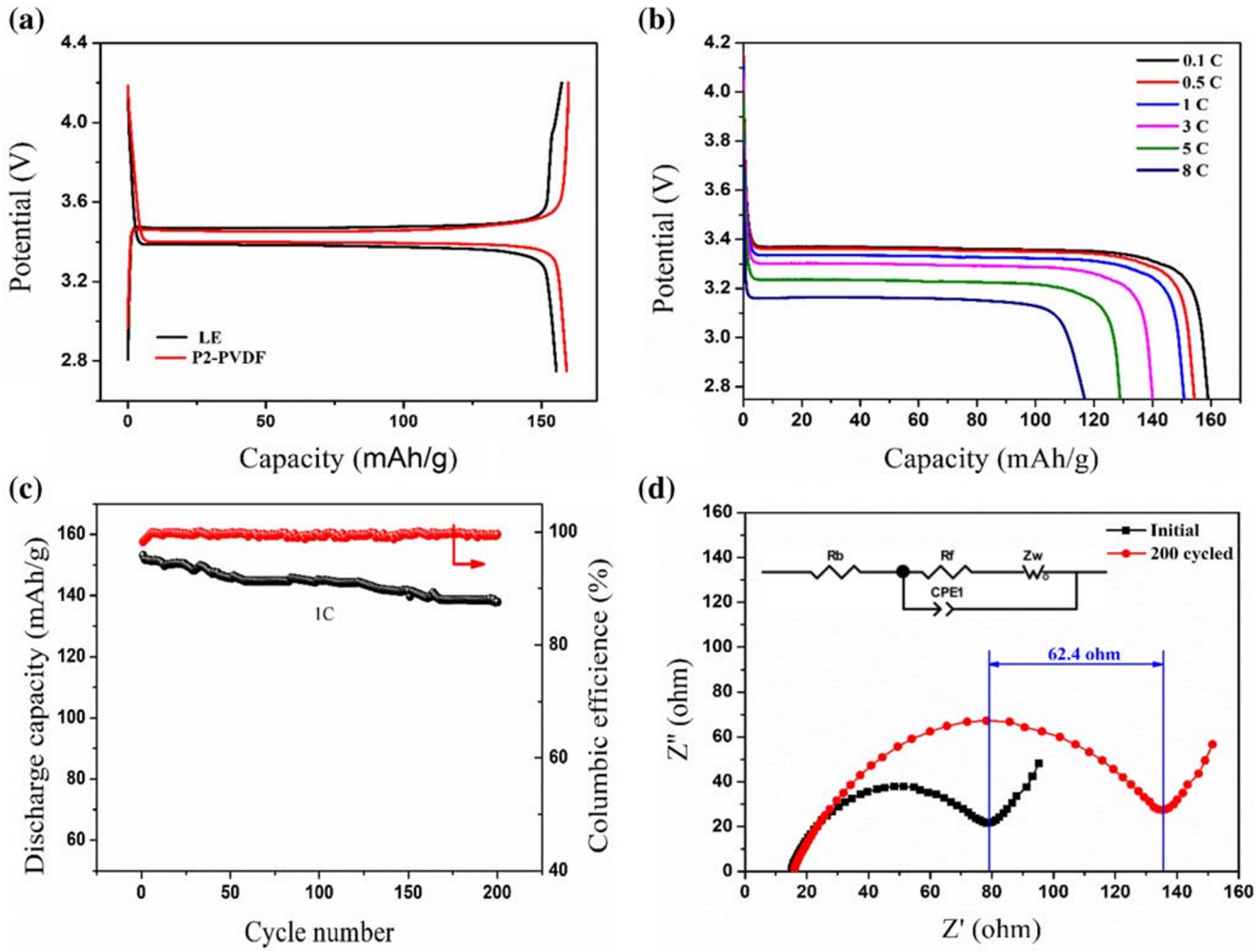

Fig. 6 The electrochemical performance of the cell **a** initial charge-discharge capacities of LE and P_2-PVDF, **b** rate behavior, **c** cycling performance at 1 °C, and **d** the resistance gap between initial and cycled

Coulobmic efficiency drops to ~ 95% with cyclic test proceeding (Fig. S4b). The remarkable electrochemical stability is attributed to robust and inhomogeneous SEI layer. For further understanding the excellent cyclic stability of the cell based on P_2-PVDF, the difference of resistance tested by EIS measurement was used to evaluate the interfacial behavior of lithium metal cells (as displayed in Fig. 6d). The fist intercept of the semicircle on the EIS plot represents the bulk resistance of cell (R_b); diameter of the semicircle gives the value of charge transfer resistance R_{ct}. As seen from Fig. 6d, R_{ct} of the cell equipping P_2-PVDF as electrolyte, corresponding to migration of lithium ion between the electrode and electrolyte interface, is only 74.3 Ω. The resistance gains to 136.7 Ω, as the cyclic numbers ended at 200 cycles. The gained resistance owes to formation of SEI layer and inevitable irreversible side reaction between bare lithium and electrolyte. The difference between initial and cycled ones determined the level of polarization [32–34]. Therefore, the resistance of P_2-PVDF compared to initial one only raises 62.4 Ω which is much lower than that of LE (183 Ω, see Fig. S4c). This small resistance indicates the cell using P_2-PVDF as electrolyte keeps a low polarization state which benefits from formation of highly homogenous SEI layer, rather than that of sustaining consumption of lithium metal to maintain intact SEI layer [35, 36].

Conclusions

In this paper, P-PVDF is prepared via one-pot synthesis strategy based on in situ polymerization of melamine and epoxy-ended amino-terminated polyoxypropylene with $LiPF_6$-based liquid electrolyte in framework of PVDF nanofiber. The polymer cross-linking PVDF nanofiber not only improves mechanical strength for polymer electrolyte but also contributes to the one-off formation of a homogenous SEI layer to suppressing dendrite lithium. The ether-dominated polymer chains provide ionic transportation channel induced high ionic conductivity (1.35 mS/cm). As consequence, the as-assembled cell presents superior electrochemical performance. In comparison with LE, the P-PVDF polymer electrolyte exhibits significantly enhanced rate behavior with retention rate of 75% (61% for the liquid electrolyte) at 8 C, cycling stability of 92% initial capacities (80% for liquid electrolyte) after 200 cycles.

Funding information This work are supported by the link projects of the National Natural Science Foundation of China (No. 11602082), Hunan Provincial Natural Science Foundation of China (No. 2019JJ50136) and the scientific research fundation of Hunan Provincial Education Department (No. 19C0596 and 19C596).

Compliance with ethical standards

Conflict of interest The authors declare that they have no conflict of interest.

References

1. Han JH, Liu P, Ito Y, Guo XW, Hirata A, Fujita T, Chen MW (2018) Bilayered nanoporous graphene/molybdenum oxide for high rate lithium ion batteries. Nano Energy 45:273–279
2. Scrosati B, Garche J (2010) Lithium batteries: status, prospects and future. J Power Sources 195:2419–2430
3. Wang B, Ryu J, Choi S, Song G, Hong D, Hwang C, Chen X, Wang B, Li W, Song HK, Park S, Ruoff RS (2018) Folding graphene film yields high areal energy storage in lithium-ion batteries. ACS Nano 12:1739–1746
4. Dumn B, Kamath H, Tarascon JM (2011) Electrical energy storage for the grid: a battery of choices. Science 334:928–935
5. Lee H, Yanilmaz M, Toprakci O, Fu K, Zhang X (2014) A review of recent developments in membrane separators for rechargeable lithium-ion batteries. Energy Environ Sci 7:232
6. Kong L, Peng HJ, Huang JQ, Zhang Q (2017) Review of nanostructure current collectors in lithium-sulfur batteries. Nano Res 10: 4027–4054
7. Chen L, Shaw LL (2014) Recent advances in lithium–sulfur batteries. J Power Sources 267:770–783
8. Woo H, Wi S, Kim J, Lee S, Hwang T, Kang J, Kim J, Park K, Gil B, Nam S, Park B (2018) Complementary surface modification by disordered carbon and reduced graphene oxide on SnO2 hollow spheres as an anode for Li-ion battery. Carbon 129:342–348
9. Zhang J, Liu Z, Kong Q, Zhang C, Pang S, Yue L, Wang X, Yao J, Cui G (2013) Renewable and superior thermal-resistant cellulose-based composite nonwoven as lithium-ion battery separator. ACS Appl Mater Interfaces 5:128–134
10. Liu T, An QF, Wang XS, Zhao Q, Zhu BK, Gao CJ (2014) Preparation and properties of PEC nanocomposite membranes with carboxymethyl cellulose and modified silica. Carbohydr Polym 106:403–409
11. Li H, Wang Z, Chen L, Huang X (2009) Research on advanced materials for Li-ion batteries. Adv Mater 21:4593–4607
12. Balke N, Jesse S, Morozovska A, Eliseev E, Chung D, Kim Y, Adamczyk L, Garcia R, Dudney N, Kalinin S (2010) Nanoscale mapping of ion diffusion in a lithium-ion battery cathode. Nat Nanotechnol 5:749
13. Huang X (2010) Separator technologies for lithium-ion batteries. J Solid State Electr 15:649–662
14. Zhu B, Liu X, Li N, Yang C, Ji T, Yan K, Chi H, Zhang X, Sun F, Sun D, Chi C, Wang X, Wang Y, Chen L, Yao L (2019) Three-dimensional porous graphene microsphere for high-performance anode of lithium ion batteries. Surf Coat Tech 360:232–237
15. Liao H, Hong H, Zhang H, Li Z (2016) Preparation of hydrophilic polyethylene/methylcellulose blend microporous membranes for separator of lithium-ion batteries. J Membrane Sci 498:147–157
16. Liao H, Zhang H, Hong H, Li Z, Qin G, Zhu H, Lin Y (2016) Novel cellulose aerogel coated on polypropylene separator as gel polymer electrolyte with high ionic conductivity for lithium-ion batteries. J Membrane Sci 514:332–339
17. Etacheri V, Marom R, Elazari R, Salitra G, Aurbach D (2011) Challenges in the devellopment of advanced Li-ion batteries: a review. Energy Environ Sci 4:3243
18. Rollins HW, Harrup MK, Dufek EJ, Jamison DK, Sazhin SV, Gering KL, Daubaras DL (2014) Fluorinated phosphazene co-solvents for improved thermal and safety performance in lithium-ion batteries electrolyte. J Power Sources 263:66–74
19. Xiao W, Wang Z, Miao C, Yan X (2016) Preparation of Si/Ti mesoporous melecular sieve and its application in P (VDF-HFP)-based composite polymer electrolytes. Electrochim Acta 216:467–474
20. Bachman JC, Muy S, Grimaud A, Chang HH, Pour N, Lux SF, Paschos O, Maglia F, Lupart S, Lamp P, Giordano L, Shao-Horn Y (2016) Inorganic solid-state electrolyte for lithium batteries:

mechanisms and properties governing ion conduction. Chem Rev 116:140–162
21. Li G, Gao Y, He X (2017) Organosulfide-plasticized solid-electrolyte interphase layer enables stable lithium metal anodes for long-cycle lithium-sulfur batteries. Nat Commun 8:850
22. Larcher D, Tarascon JM (2015) Towards greener and more sustainable batteries for electrical energy storage. Nat Chem 7:19–29
23. Watanable M, Thomas ML, Passerini S (2017) Ionic-liquid based polymer electrolyte liquids to energy storage and conversion materials and devices. Chem Rev 117:7190–7239
24. Zhao Q, Xie R, Luo F, Faraj Y, Liu Z, Ju XJ, Wang W, Chu LY (2018) Preparation of high strength poly (vinylidene fluoride) porous membrane with cellular structure via vapor-induced phase separation. J Membrane Sci 549:151–164
25. Xia Y, Liang YF, Xie D, Wang XL, Zhang SZ, Xia XH, Gu CD, Tu JP (2019) A poly (vinylidene fluoride-hexafluoropropylene) based three-dimensional network gel polymer electrolyte for solid-state lithium-sulfur batteries. Chem Eng J 358:1047–1053
26. Zhu Y, Wang F, Liu L, Xiao S, Chang Z, Wu Y (2013) Composite of a nonwoven fabric with poly (vinylidene fluoride) as a gel membrane of high safety for lithium ion battery. Energy Environ Sci 6: 618–624
27. Liao H, Zhang H, Qin G, Li Z, Li L, Hong H (2017) A macroporous graphene oxide-based membrane as a separator with enhanced thermal stability for high-safety lithium-ion batteries. RSC Adv 7:22112–22120
28. Kim YB, Tran-Phu T, Kim M, Jung DW, Yi GR, Park JH (2015) Facilitated ion diffusion in multiscale porous particles: application in battery separators. ACS Appl Mater Interfaces 7:4511–4517
29. Ryou MH, Lee YM, Park JK, Choi JW (2011) Mussel-inspired polydopamine-treated polyethylene separators for high-power li-ion batteries. Adv Mater 23:3066–3070
30. Fang L-F, Shi J-L, Zhu B-K, Zhu L-P (2013) Facile introduction of polyether chains onto polypropylene separators and its application in lithium ion batteries. J Membrane Sci 448:143–150
31. Liao H, Chen H, Zhou F, Zhang Z, Chen H (2019) Dendrite-free lithium deposition induced by mechanical strong sponge-supported unique 3D cross-linking polymer electrolyte for lithium metal batteries. J Power Sources 435:226748
32. Eo S-M, Cha E, Kim D-W (2009) Effect of an inorganic additive on the cycling performances of lithium-ion polymer cells assembled with polymer-coated separators. J Power Sources 189:766–770
33. Kim JY, Lim DY (2010) Surface-modified membrane as a separator for lithium-ion polymer battery. Energies 3:866–885
34. Park J-H, Cho J-H, Park W, Ryoo D, Yoon S-J, Kim JH, Jeong YU, Lee S-Y (2010) Close-packed SiO2/poly (methyl methacrylate) binary nanoparticles-coated polyethylene separators for lithium-ion batteries. J Power Sources 195:8306–8310
35. Zhou D, Shanmukaraj D, Tkacheva A, Armand M, Wang G (2019) Polymer electrolytes for lithium-based batteries: advances and prospects. Chem 5:2326–2352
36. Zhou D, Tkacheva A, Tang X, Sun B, Shanmukaraj D, Li P, Zhang F, Armand M, Wang G (2019) Stable conversion chemistry-based lithium metal batteries enabled by hierarchical multifunctional polymer electrolytes with near-single ion conduction. Angew Chem Int Ed 58:6001–6006